Journal of
Micro/Nanolithography, MEMS, and MOEMS

SPIEDigitalLibrary.org/jm3

Simultaneous detection of multiple biological targets using optimized microfluidic microsphere-trap arrays

Xiaoxiao Xu
Zhenyu Li
Pinaki Sarder
Nalinikanth Kotagiri
Arye Nehorai

SPIE

Simultaneous detection of multiple biological targets using optimized microfluidic microsphere-trap arrays

Xiaoxiao Xu,[a] Zhenyu Li,[b] Pinaki Sarder,[c] Nalinikanth Kotagiri,[c] and Arye Nehorai[a,*]
[a]Washington University in St. Louis, Preston M. Green Department of Electrical and Systems Engineering, One Brookings Drive, St. Louis, Missouri 63130
[b]George Washington University, Department of Electrical and Computer Engineering, 2121 I Street NW, Washington, DC 20052
[c]Washington University School of Medicine in St. Louis, Mallinckrodt Institute of Radiology, 660 S. Euclid Avenue, St. Louis, Missouri 63110

Abstract. We propose an analytical framework to build a microfluidic microsphere-trap array device that enables simultaneous, efficient, and accurate screening of multiple biological targets in a single microfluidic channel. By optimizing the traps' geometric parameters, the trap arrays in the channel of the device can immobilize microspheres of different sizes at different regions, obeying hydrodynamically engineered trapping mechanism. Different biomolecules can be captured by the ligands on the surfaces of microspheres of different sizes. They are thus detected according to the microspheres' positions (position encoding), which simplifies screening and avoids target identification errors. To demonstrate the proposition, we build a device for simultaneous detection of two target types by trapping microspheres of two sizes. We evaluate the device performance using finite element fluidic dynamics simulations and microsphere-trapping experiments. These results validate that the device efficiently achieves position encoding of the two-sized microspheres with few fluidic errors, providing the promise to utilize our framework to build devices for simultaneous detection of more targets. We also envision utilizing the device to separate, sort, or enumerate cells, such as circulating tumor cells and blood cells, based on cell size and deformability. Therefore, the device is promising to become a cost-effective and point-of-care miniaturized disease diagnostic tool. [DOI: 10.1117/1.JMM.13.1.013017]

Keywords: microfluidics; microsphere-trap arrays; simultaneous detection; multiple targets.

Paper 14006P received Jan. 14, 2014; revised manuscript received Feb. 24, 2014; accepted for publication Mar. 4, 2014; published online Mar. 26, 2014.

1 Introduction

Microsphere arrays can be used to effectively detect and quantify biological targets, such as proteins and mRNAs, which are key biomolecules for maintaining normal physiological and molecular activities in cells and organs. In the microsphere arrays, the microspheres are functionalized with ligands on their surface that are specific to certain targets.[1–4] These arrays have great potential such as the independent, quantitative, and simultaneous assay of multiple types of targets in small volumes of material and collection of statistically rigorous data from numerous microspheres for each type of target. Recently, integrating microfluidics technology with the microsphere arrays has aroused great interest. The integrated microfluidic microsphere array systems have many advantages such as offering a controlled liquid environment, reducing reagent cost and hybridization assay time, and providing the potential for mass production of devices at low cost.[5,6] Therefore, these systems have played an increasingly important role in life science research and medical diagnostics.

To simultaneously detect and correlate multiple targets, researchers have designed advanced array systems. To identify the different targets on the microspheres, Luminex's suspension array technology sorts microspheres based on their colors,[4] Illumina's bead array systems utilize complex protocol and setup to code and decode the microspheres,[7] and label-based approaches rely on different labels (e.g., fluorescent dyes at distinct emission wavelengths) on the targets.[2] In these approaches, the microspheres are randomly suspended or placed so that the captured different targets are mixed. As a result, subsequent imaging and data analysis require complex segmentation of the microspheres, and the noise in the imaging makes the analysis even more prone to errors in identifying the targets.[8–10] To solve the limitations of these label-based approaches, we have previously designed a microsphere array device with microspheres immobilized at predetermined locations (i.e., position encoding) in a highly parallel and compact fashion.[1] Then, target identification can be achieved according to the precise positioning of the microspheres, which simplifies the image analysis and is error-free. For simultaneous detection of multiple targets, one possibility is to implement multiple channels connected with individual chambers on a microfluidic chip and to use on-chip valves to open or lock the channels to direct the microspheres for a specific type of targets to flow into a specific chamber.[11–16] While this approach can achieve multiplexing, a disadvantage is that the valves occupy a lot of space on the chip and most of the on-chip valves need a sophisticated external actuation platform supplied by a control and actuation system.[17] Moreover, for effective collection of information, such as profiling multiple proteins or simultaneous mRNA and protein profiling, and for precise flow condition and local environment control, there is a need for multianalyte detection in a single microfluidic channel. Therefore, we aim to develop a simple, easy-to-control, and efficient one-channel platform for simultaneous detection and quantification of multiple targets.

*Address all correspondence to: Arye Nehorai, E-mail: nehorai@ese.wustl.edu

0091-3286/2014/$25.00 © 2014 SPIE

In this article, to achieve simultaneous and efficient detection of multiple targets by position encoding in a single-channel device, we design the trap arrays by proposing a simple but effective idea.[18] Specifically, we propose microspheres of different sizes to capture different targets. We select the geometric parameters of the traps to separate and immobilize the different microspheres at different known regions in the same channel by microfluidic hydrodynamic trapping,[19] without using different channels (chambers) and on-chip valves. Finally, as stated, the targets are captured by the microspheres and detected according to their positions.[1] To optimize the performance of our proposed device, we compute the values of the trap arrays' geometric parameters by extending our previous optimization framework for designing a single-target detection device.[20] Besides the extension, the adopted optimization constraints from previous framework are also modified to consider more experimental conditions such as the variations of the microspheres' sizes and device fabrication. To demonstrate the design, we fabricate a device for simultaneous detection of two types of targets by trapping microspheres of two sizes. We validate the design through finite element fluidic dynamics simulations and also by using microsphere-trapping experiments on the fabricated device. The results show that the device achieves the position encoding of the microspheres with few fluidic errors, providing the promise to utilize our framework to build devices for simultaneous detection of more targets. We envision that the device can be utilized to separate, sort, or enumerate cells, including circulating tumor cells and blood cells, based on cell size and deformability.[21–24] To achieve these goals, however, further development of the device is required to solve issues such as blood clogging. Overall, our device for simultaneous detection of multiple targets in a single channel improves information gathering efficiency, reduces fabrication complexity, and is promising to become a fast and cheap disease diagnostic tool.

This article is organized as follows. In Sec. 2, we describe the design strategy of the microsphere-trap arrays for simultaneous detection of multiple targets. We then present the optimization framework to select the device's trap geometry. In Sec. 3, to demonstrate our design, we compute the geometric parameters of a device for detecting two types of targets. We then provide finite element fluidic dynamics simulation and experiment validation for the device, both of which show that the device works well with superior performance. Section 4 provides the concluding remarks.

2 Methods

2.1 *Design Strategy*

The design of the microfluidic microsphere array platform for simultaneous detection of multiple targets in a single channel is based on our previous work in which we proposed and implemented a microfluidic microsphere-trap array device to capture uniform-sized microspheres.[20] Here, we briefly describe the general configuration of the device, as shown in the schematic of Fig. 1. The trap arrays, consisting of inverted-trapezoid grooves, are made of polydimethylsiloxane (PDMS). Each row of the trap arrays is offset horizontally with respect to the one ahead. The platform has an inlet and an outlet to let through a fluidic stream. The microspheres with specific ligands are contained in the stream and are immobilized in the traps by hydrodynamic trapping mechanism when the stream flows through the channel.

The microfluidic microsphere-trap array device employs fluidic resistance and path engineering to perform precise hydrodynamic trapping of the microspheres. A microsphere in the stream has two possible flow paths: trapping path P_1 or bypassing path P_2 (see Fig. 1). Here, trapping is defined as the flow of a microsphere into a trap, and bypassing is defined as the subsequent microspheres flowing through the trap's neighboring gaps. The geometry of the trap arrays is designed that a microsphere experiences a lower flow resistance in the trapping path P_1 for an empty trap than it does in the bypassing path P_2. Thus, the microsphere has a higher chance to follow P_1 to fill the empty trap. Once a trap is filled, the corresponding flow path P_1 is almost blocked and its flow resistance dramatically increases to be much greater than that in P_2. Therefore, the subsequent microspheres follow path P_2 and get immobilized by other traps downstream.

For a simple and simultaneous screening of multiple types of targets in a single channel, we employ microspheres of different sizes to capture different targets. We design the geometric parameters of the traps to immobilize the different-sized microspheres at different known regions on a single channel. Particularly, from the inlet to the outlet in the chip, the arrays of the largest traps are located nearest to the inlet, the upper and bottom openings of which are optimized to trap the largest microspheres and let through the other smaller microspheres. The arrays of the second-largest traps followed the largest trap arrays, which are designed to trap the second-largest microspheres and let through the remaining smaller microspheres. Then, the arrays of the third-largest traps are located, so on and so forth. The trapping of the different-sized microspheres during the experiment is in the reverse order. We first load the fluidic stream containing the smallest microspheres, which are to be immobilized by the smallest trap arrays at the bottom of the channel. Then, we load the second-smallest microspheres until all different-sized microspheres are immobilized at their corresponding regions. The targets, either tagged on the microspheres before loading or tagged on the immobilized microspheres in the traps through on-chip reaction, will be identified by positions of their tagged microspheres (position encoding).[1] The targets are further quantified by subsequent microscopy imaging. We note that to avoid the overload of these microspheres, their concentrations should be carefully controlled so that the number of microspheres is less than the numbers of their corresponding traps.

To optimize the device performance, in our previous work implementing the microfluidic microsphere-trap array device to capture uniform-sized microspheres,[20] we developed an analytical method to optimize the values of the trap array geometric parameters. This optimization maximized the microsphere arrays' packing density to make the device compact. It simultaneously also satisfied other criteria such as efficient microsphere trapping, minimum fluidic errors, such as channel clogging and multiple microspheres in a single trap, a feasible fabrication, and minimum errors induced during the subsequent fluorescence imaging.

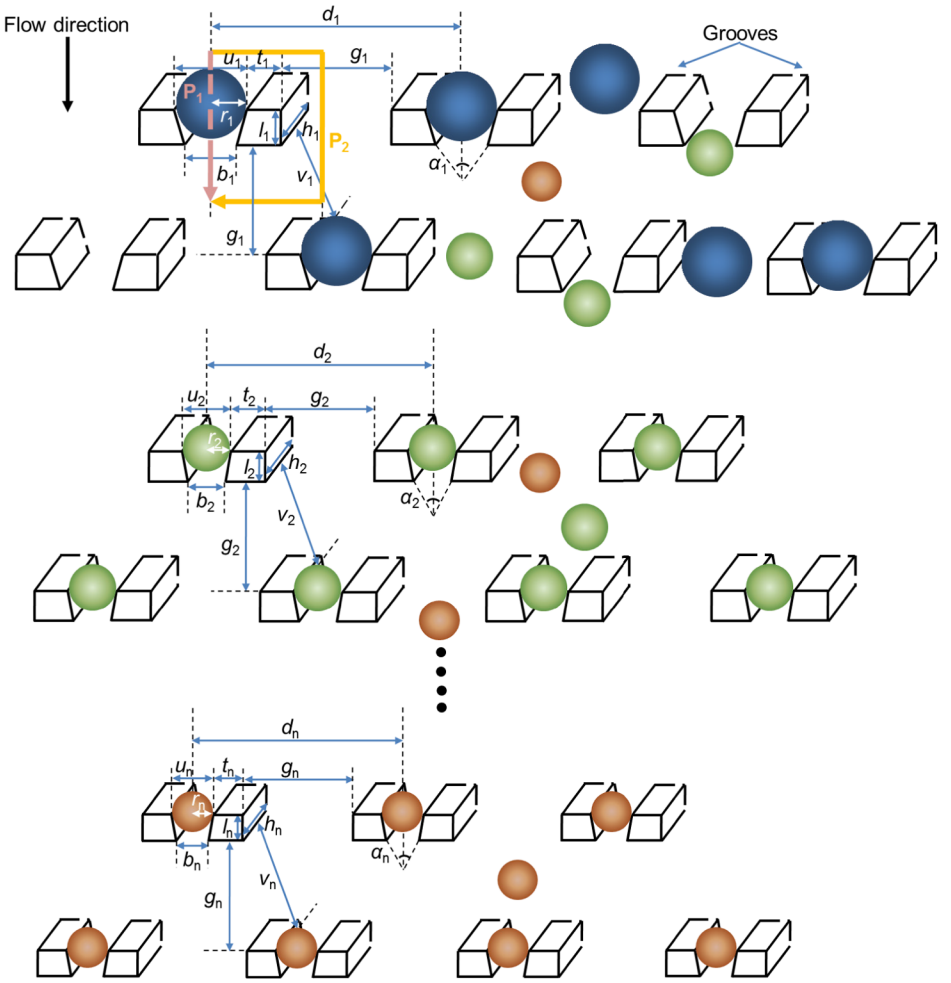

Fig. 1 Schematic diagram of microfluidic microsphere-trap array geometries for simultaneous detection of multiple types of targets. Microspheres of distinct sizes (shown in blue, green, and orange colors) are encoded with different specific receptors (not shown) to capture different types of targets. The corresponding trap arrays for immobilizing the microspheres are presented here with two adjacent rows for microspheres of each size. From the inlet to the outlet, the arrays of the largest traps are located nearest to the inlet, to trap the largest microspheres and let through the other smaller microspheres. The arrays of the second-largest traps followed the largest trap arrays, to trap the second-largest microspheres and let through the remaining smaller microspheres, so on and so forth.

Microsphere-trapping experiments showed that the optimized device greatly outperforms the unoptimized device. Here, to optimize the geometric parameters for our multiple target detection device, we extend and modify the optimization framework by revising the objective function and adding constraints to satisfy the design strategy. Besides the extension, we also consider more constraints involving experimental conditions such as the variations of the microspheres' sizes and device fabrication. The next subsection gives the details of the optimization of our design.

2.2 *Optimization of the Trap Geometry*

Here, we present the formulation of the optimal design, including the optimization objective and constraints, for our microfluidic microsphere-trap arrays for simultaneous detection of multiple targets. In Fig. 1, we show the schematic of the trap array geometries and depict the corresponding geometric parameters. Microspheres of n distinct sizes (for demonstration, three sizes are presented in blue, green, and orange colors) are encoded with n specific ligands (not shown) to capture n types of targets. For the microsphere of the i'th largest ($i = 1, \ldots, n$) size and its corresponding traps, we first define r_i as the microsphere radius. However, due to the manufacturing limitation, the sizes of the microspheres used in experiments are not perfectly uniform but have some variations. In other words, the radius of the i'th microsphere is a random variable R_i, with its mean $\mathbb{E}[R_i]$ and standard deviation $\sigma[R_i]$ are provided by the manufacturing company. We also define h_i as the trap groove walls' height, l_i and t_i as the groove walls' length and upper width, u_i and b_i as the trap opening upper and bottom widths, and α_i as the trap trapezoid angle. We further define g_i as the gap width between two traps in the same row, v_i as the distance between a trap groove wall and a microsphere filled in a trap in the next row, and d_i as the distance between two immobilized microspheres in the same row. We finally define for the i'th microsphere, S_i as a single trap and surrounding area, and ρ_i as the corresponding trap arrays' packing density.

Now, we present our optimization framework to obtain the optimal geometric parameters of the trap arrays for

microspheres of n sizes. The optimization objective is to maximize the packing density ρ_i, $i = 1, \ldots, n$, for each trap region, which is equivalent to minimizing the area S_i with the geometric parameters $\boldsymbol{\delta}_i = [R_i, h_i, l_i, u_i, b_i, t_i, g_i, d_i, v_i]^T$. To summarize, the optimization problem is

$$\rho_{i,\text{opt}} = 1/S_{i,\text{opt}}, \quad \text{with} \quad S_{i,\text{opt}} = \min_{\delta_i}(g_i + l_i) \cdot (u_i + 2t_i + g_i), \tag{1}$$

where $\boldsymbol{\delta}_i \in \{C_{i1} \cap C_{i2} \cap C_{i3} \cap C_{i4} \cap C_{i5} \cap C_{i6} \cap C_{i7} \cap C_{i8}\}$ and C_{ij}, $j = 1, \ldots, 8$ are the optimization constraints providing the feasible parameter spaces for the i'th microspheres and traps. We note that the constraints C_{i1}, C_{i5}, and C_{i6} are adapted from our previous optimization framework,[20] C_{i2} to C_{i4} are modified to consider the randomness of microsphere size and fabrication variation, and C_{i7} and C_{i8} are specifically proposed to achieve the simultaneous detection of multiple targets. Details are given below

- Constraint C_{i1} is to ensure the hydrodynamic trapping. That is, the trap array geometry is designed so that path P_1 (pink line in Fig. 1) for an empty trap has a lower flow resistance than path P_2 (green line in Fig. 1). Then, the microsphere in the fluid through the channels chooses path P_1 to move into an empty trap. However, once the trap through P_1 is filled by a microsphere, the flow resistance in P_1 increases and becomes larger than that in P_2. Thus, subsequent microspheres divert to path P_2 and bypass the filled trap. The specific representation of C_{i1} is adapted from Eq. (7) in our previous optimization framework.[20]
- Constraint C_{i2} is to ensure a single microsphere in each trap and to avoid multiple microspheres trapped at one trap location. We require that the trap opening bottom width b_i be smaller than the microsphere diameter ($b_i < 2R_i$) and that the trap opening upper width u_i and the groove wall length l_i be smaller than the sum of two microsphere diameters ($u_i < 4R_i$, $l_i < 4R_i$). Because R_i is a random variable and is not present in the objective function, these constraints can be written in a probabilistic form.[25] For example, the probabilistic constraint for b_i is $\text{Prob}\{b_i < 2R_i\} \geq q$, with q as the probability that is usually selected close to 1. Because the number of microspheres is usually large and the mean $\mathbb{E}[R_i]$ and standard deviation $\sigma[R_i]$ of the microsphere's radius can be obtained from the manufacturing company, we assume that the R_i follows a normal distribution by central limit theorem.[26] Therefore, the constraint for b_i is rewritten as $b_i < 2(\mathbb{E}[R_i] - \Phi^{-1}(q)\sigma[R_i])$, where $\Phi^{-1}(\cdot)$ is the quantile function (cumulative distribution function) of the standard normal distribution. Similarly, we rewrite the probabilistic constraints for u_i and l_i as $u_i < 4(\mathbb{E}[R_i] - \Phi^{-1}(q)\sigma[R_i])$ and $l_i < 2(\mathbb{E}[R_i] - \Phi^{-1}(q)\sigma[R_i])$, respectively. Finally, we consider possible fabrication variations and add 0.2-μm safety margins.[27] Therefore, constraint C_{i2} is

$$\begin{aligned} C_{i2} = \{&b_i \leq 2(\mathbb{E}[R_i] - \Phi^{-1}(q)\sigma[R_i]) - 0.2, \\ &u_i \leq 4(\mathbb{E}[R_i] - \Phi^{-1}(q)\sigma[R_i]) - 0.2, \\ &l_i \leq 4(\mathbb{E}[R_i] - \Phi^{-1}(q)\sigma[R_i]) - 0.2\}. \end{aligned} \tag{2}$$

- Constraint C_{i3} is to ensure that a microsphere is stably immobilized in a trap and is not swept away by the transient fluid flow around it. This constraint is given by constraining the trapezoid angle α_i to be greater than 5 deg $\{\alpha_i = 2 \arctan[0.5(u_i - b_i)/l_i] \geq 5 \text{ deg}\}$ and the groove wall length l_i to be greater than the microsphere's radius ($l_i > R_i$). Similar to constraint C_{i2}, we consider the randomness of R_i and the safety margin, and C_{i3} becomes

$$\begin{aligned} C_{i3} = \{&-\alpha_i \leq -5 \text{ deg}, -l_i \\ &\leq -(\mathbb{E}[R_i] + \Phi^{-1}(q)\sigma[R_i]) - 0.2\}. \end{aligned} \tag{3}$$

- Constraint C_{i4} is to avoid the channel clogging. We require the gap width g_i between two traps in the same row to be greater than one microsphere's diameter ($g_i > 2R_i$) and to be smaller than the sum of two microspheres' diameters ($g_i < 4R_i$). We also require the distance v_i between a trap groove wall and a microsphere filled in a trap in the next row to be greater than one microsphere's diameter [$v_i > 2R_i$, where $v_i = \sqrt{(g_i - R_i)^2 + (0.5g_i)^2}$]. Again, considering the variations of microsphere size and fabrication, C_{i4} becomes

$$\begin{aligned} C_{i4} = \{&g_i \leq 4(\mathbb{E}[R_i] - \Phi^{-1}(q)\sigma[R_i]) - 0.2, \\ &-g_i \leq -2(\mathbb{E}[R_i] + \Phi^{-1}(q)\sigma[R_i]) - 0.2, \\ &-v_i \leq -2(\mathbb{E}[R_i] + \Phi^{-1}(q)\sigma[R_i]) - 0.2\}. \end{aligned} \tag{4}$$

- Constraint C_{i5} is to ensure a feasible fabrication, i.e., the device geometric aspect ratios (the ratio of transverse dimensions to trap groove wall height, e.g., t_i/h_i) should be limited in the range of [0.4, 2.5]. This constraint is given by

$$\begin{aligned} C_{i5} = \{&l_i/h_i, g_i/h_i, b_i/h_i, u_i/h_i, t_i/h_i \leq 2.5, -l_i/h_i, \\ &-g_i/h_i, -b_i/h_i, -u_i/h_i, -t_i/h_i \leq -0.4\}. \end{aligned} \tag{5}$$

- Constraint C_{i6} is to satisfy the minimal distance $d_{i,\text{opt}}$ between microspheres obtained in the statistical design to minimize the image analysis error,[28,29] i.e., the distance d_i ($d_i = u_i + 2t_i + g_i$) between two immobilized microspheres in the same row should be greater than $d_{i,\text{opt}}$. Therefore, C_{i6} is

$$C_{i6} = \{-d_i \leq -d_{i,\text{opt}}\}. \tag{6}$$

- Constraint C_{i7}: in our design strategy, we expect the i'th microspheres to be immobilized by the i'th traps, whereas the $(i+1)$'th microspheres flow through the channels or the openings of the first to i'th traps and then are immobilized by the $(i+1)$'th traps. This requirement adds one constraint (C_{i7}) in the optimization of the geometric parameters, i.e., the bottom width of the i'th trap opening b_i should be larger than the diameter of the $(i+1)$'th microsphere ($b_i > 2R_{i+1}$). Therefore,

$$C_{i7} = \{-b_i \leq -2(\mathbb{E}[R_{i+1}] + \Phi^{-1}(q)\sigma[R_{i+1}]) - 0.2\}. \tag{7}$$

- Constraint C_{i8}: though the concentrations of the microspheres are carefully controlled to ensure that the microspheres of each size will be fully immobilized at their corresponding region, there might be excess $(i-1)$'th microspheres flowing into the i'th trap region in the worst case. We assume that the i'th trap region is long enough that the excess $(i-1)$'th microspheres will not flood into the $(i+1)$'th trap region. To avoid the channel clogging by the $(i-1)$'th microspheres, we add one constraint C_{i8} on the gap width g_i and the distance v_i with respect to the $(i-1)$'th microspheres' radius R_{i-1}, i.e.,

$$C_{i7} = \{-b_i \le -2(\mathbb{E}[R_{i+1}] + \Phi^{-1}(q)\sigma[R_{i+1}]) - 0.2, \\ -v_i \le -2(\mathbb{E}[R_{i-1}] + \Phi^{-1}(q)\sigma[R_{i-1}]) - 0.2\}. \quad (8)$$

Therefore, given the number of target types n and the radii ($\mathbb{E}[R_i]$, $\sigma[R_i]$, $i = 1, \ldots, n$) of the microspheres to capture the targets, we can obtain the geometric parameters $\boldsymbol{\delta}_i$ $(i = 1, \ldots, n)$ of our device by solving the optimization problems in Eqs. (1)–(8). We apply the grid-search method[30] to solve $\boldsymbol{\delta}_i$ $(i = 1, \ldots, n)$.

3 Results and Discussion

To demonstrate the applicability of the proposed design strategy, we build a device for detecting two types of targets. To validate the device, we use COMSOL Multiphysics 4.3 (Ref. 31) to perform finite element fluidic dynamics simulations of sequential loading of the microspheres of two sizes. To further evaluate the performance of the device, we fabricate the device and perform a number of microsphere sequential loading and trapping experiments on it.

3.1 *Optimized Device for Simultaneous Detection of Two Targets*

Based on the optimization formulation, we compute the optimal geometric parameters of the trap arrays for immobilizing microspheres of two different sizes ($n = 2$) for the demonstration of our design in finite element fluidic dynamics simulations and experiments. To tolerate manufacture variations on the two sizes of the microspheres, the values of their radii should be selected to be sufficiently distinct from each other; we use microspheres of radius $\mathbb{E}[R_1] = 7.725$ and $\mathbb{E}[R_2] = 5.055$ μm (Bangs Lab, Fishers, Indiana) with corresponding standard deviations $\sigma[R_1] = 0.55$ and $\sigma[R_2] = 0.3515$ μm, respectively. We set the probability $q = 90\%$, i.e., considering the randomness of the microsphere size, and we require the constraints to be satisfied for 90% of the time. For simplicity, we keep the values of the trap groove walls' heights h_1 and h_2 fixed. To further simplify the chip fabrication, we assign the same value to h_1 and h_2 ($h_1 = h_2 = h$). The heights should be designed shallow enough to prevent the stacking of multiple microspheres at a single trap. The heights should also be deep enough to avoid the microsphere flowing out of the channel. Here, according to the experimental testing, we choose $h \approx 2.2\mathbb{E}[R_1] \approx 3.3\mathbb{E}[R_2] = 16.5\,\mu$m. Furthermore, the minimal distances $d_{1,\text{opt}}$ and $d_{2,\text{opt}}$ to minimize the imaging errors for microspheres of radii $\mathbb{E}[R_1]$ and $\mathbb{E}[R_2]$ are 30 and 20 μm, respectively.[28] We further denote the remaining parameters in $\boldsymbol{\delta}_1$ and $\boldsymbol{\delta}_1$ as the optimization parameters. The values of these optimization parameters are solved and summarized in Table 1 (the parameters d_1, d_2, v_1, and v_2 are not listed, as they are functions of the other parameters).

3.2 *Finite Element Fluidic Dynamics Simulations*

Because three-dimensional (3-D) fluidic dynamics simulations are prohibitively computationally expensive, we perform two-dimensional (2-D) simulations. The accuracy of the 2-D time-dependent simulations of the hydrodynamic trapping of microspheres has been validated by experiments in our previous publication.[31] One can refer to it for more details to build the finite element simulation model. In the simulations, we precisely consider the geometric parameters of the microspheres and the trap arrays as presented in Table 1. Recall that the microspheres of different sizes are loaded sequentially to simplify the operation; therefore, we perform our simulations by first loading the small microspheres and then loading the large microspheres.

Figures 2 and 3 present the positions of the microspheres, as well as the fluid velocity magnitude distributions and fluid directions, at several time points. Figure 2 shows that the small microspheres flow through the large trap array region, into the small trap array region, and are finally immobilized by their corresponding small traps. Figure 3 demonstrates that the large microspheres flow into the large trap region and are immobilized by their corresponding large traps. These finite element simulation results verify the applicability of the device design strategy for simultaneous detection of two types of targets.

Table 1 Fixed and optimization geometric parameters for the microfluidic microsphere-trap arrays for simultaneous detection of two types of targets.

	$\mathbb{E}[R_1]$	$\mathbb{E}[R_2]$	$\sigma[R_1]$	$\sigma[R_2]$	h_1	h_2
Fixed values (μm)	7.725	5.055	0.55	0.3515	16.5	16.5
Optimized values for the large microsphere-trap arrays (μm)	$l_{1,\text{opt}}$	$u_{1,\text{opt}}$	$b_{1,\text{opt}}$	$t_{1,\text{opt}}$	$g_{1,\text{opt}}$	$s_{1,\text{opt}}$
	8.62	15.18	11.88	6.60	25.73	1859.3 (μm^2)
Optimized values for the small microsphere-trap arrays (μm)	$l_{2,\text{opt}}$	$u_{2,\text{opt}}$	$b_{2,\text{opt}}$	$t_{2,\text{opt}}$	$g_{2,\text{opt}}$	$S_{2,\text{opt}}$
	6.60	9.90	6.93	6.60	19.36	1102.2 (μm^2)

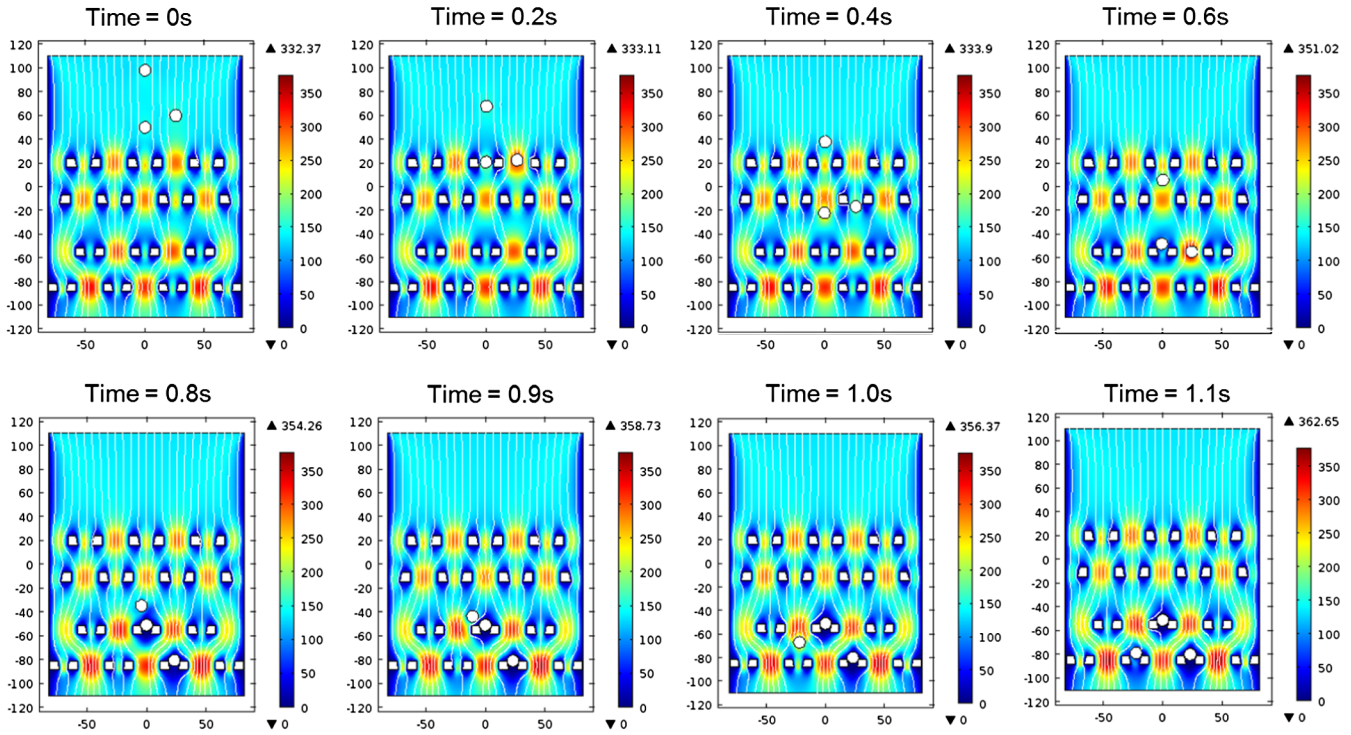

Fig. 2 Finite element fluidic dynamics simulation of small microspheres flowing in the device for detecting two types of targets. The streamlines indicate the flow direction, and the rainbow color represents the flow-velocity magnitude distribution (μm/s) with a fixed value range for all plots. The three small microspheres flow through the large trap array region, into the small trap array region, and are finally immobilized by their corresponding small traps.

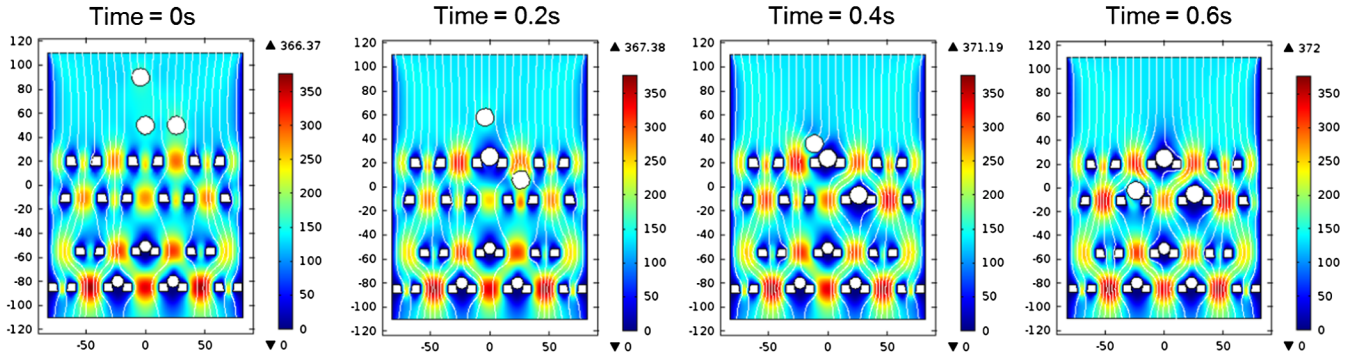

Fig. 3 Finite element fluidic dynamics simulation of large microspheres flowing in the device for detecting two types of targets. The streamlines indicate the flow direction, and the rainbow color represents the flow-velocity magnitude distribution (μm/s) with a fixed value range for all plots. The three large microspheres flow into the large trap array region and are immobilized by their corresponding large traps.

The simulations show the sequential loading and trapping processes of only two-sized microspheres. In the sequential loading, there is no difference between simulations of microspheres of two or more sizes, because the smallest microspheres are loaded and trapped first, then the second smallest microspheres, so on and so forth. Therefore, to comply with our experiments in the next subsections, we present the simulations of two-sized microspheres here.

3.3 *Device Fabrication and Operation*

The microsphere-trap array chip was connected by an inlet and an outlet to the external world [Fig. 4(b)]. The optimized chip has a width of 1000 μm and a length of 1000 μm. The device, made of PDMS, was fabricated by using soft lithography techniques.[16] We first fabricated a master SU8-3025 mold on a 3-in. silicon wafer using conventional photolithography. Then, PDMS prepolymer (RTV615) was mixed at 10:1 A:B ratio and poured onto the mold. It was degassed in a vacuum chamber and was then cured in an 80°C oven for 30 min. Then, we peeled the partially cured PDMS off from the mold and punched liquid inlet and outlet ports through the whole layer using a 0.75-mm diameter biopsy punch. Finally, the PDMS layer with fluidic pattern was permanently bonded to a standard glass slide after air plasma treatment. The master molds could be reused many times.

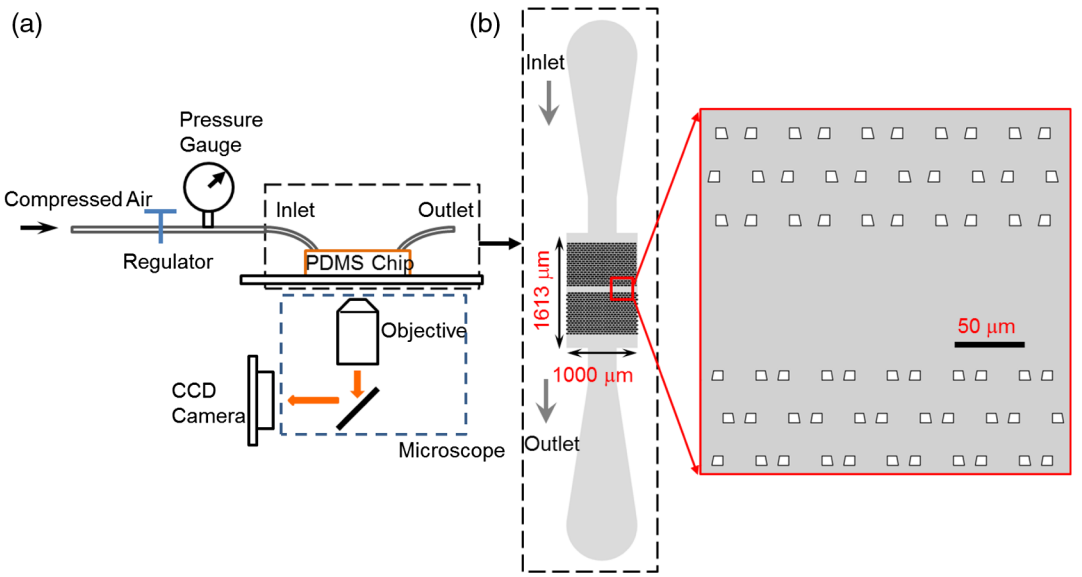

Fig. 4 (a) Schematic diagram of the experimental setup. (b) Layout (top view) of the microfluidic microsphere-trap array for simultaneous detection of two types of targets.

Figure 4(a) shows the experimental setup. The device was mounted on an inverted fluorescent microscope [Olympus IX71 (Center Valley, Pennsylvania) equipped with an EMCCD camera (Andor iXon+)]. Two solutions of polystyrene microspheres (7.725- and 5.055-μm mean radii, Bangs Lab), with concentrations of 5×10^4/mL, were prepared in 1× PBS buffer with 0.05% Tween-20 (Sigma Aldrich, St. Louis, Missouri). First, the 5-μm microsphere solution was loaded into a 22-gauge Tygon tubing (Cole Parmer, Vernon Hills, Illinois). The device input port connected one end of the tubing via a stainless steel tube. A compressed N_2 pressure source controlled by a pressure regulator with a resolution of 0.1 psi connected the other end of the tubing and pushed the microsphere solution into the device by applying 1 psi pressure to the tubing. After loading the 5-μm microspheres, the same loading procedure was repeated with a 7.7-μm microsphere solution to complete the loading process. The EMCCD camera captured the snapshots and videos of the experimental process.

3.4 *Experimental Results*

We present the experimental results using the fabricated device to sequentially trap microspheres of mean radii 5.055 and 7.725 μm. Figure 5 presents the snapshots after the 5-μm microsphere loading process [Fig. 5(a)] and after the 7.7-μm microsphere loading process [Fig. 5(b)]. The videos showing the two loading processes are in Video 1 and 2. The 5-μm traps are located after the 7.7-μm ones to avoid 7.7-μm microspheres trapped at the 5-μm locations. However, 7.7-μm microsphere overflow to the 5-μm traps can still occur if too many 7.7-μm microspheres are loaded into the device. Therefore, it is preferable to load the 5-μm microspheres first, so that even when the 7.7-μm

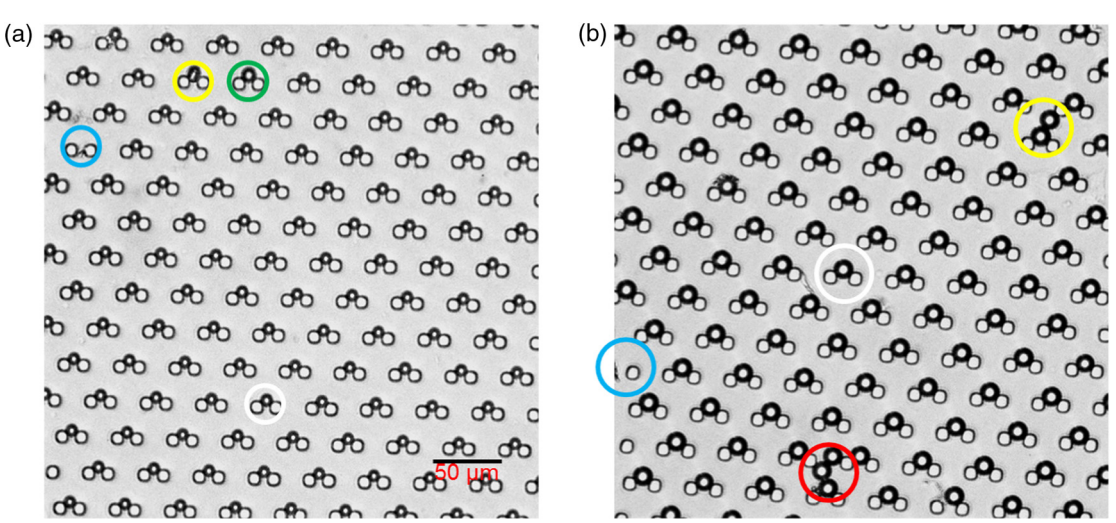

Fig. 5 Camera snapshots at the end time points of (a) the 5-μm microsphere loading process and (b) the 7.7-μm microsphere loading process. Highlighted areas of trapping results: single (white circle), multiple (yellow circle), empty (blue circle), clogged (red circle), and wrong-trapped (green circle).

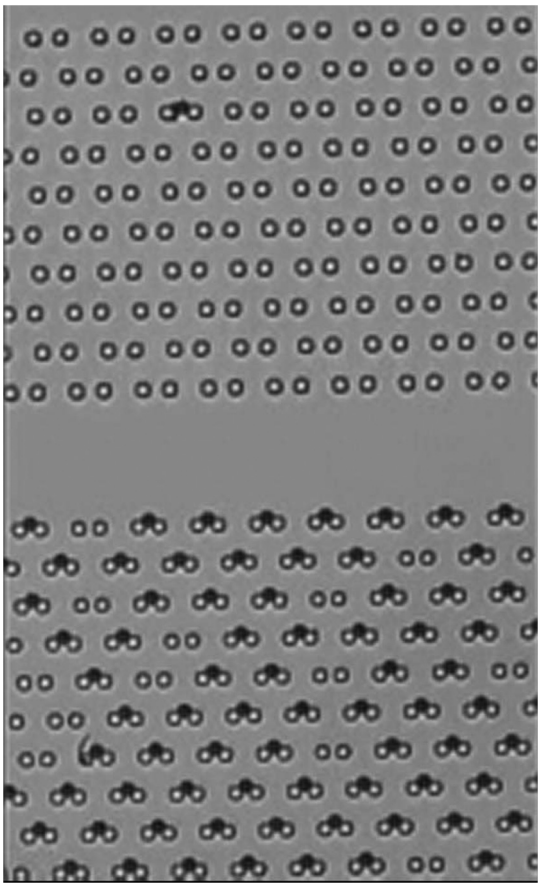

Video 1 The trapping processing of the small microspheres into the small trap region (MPEG, 2.69 MB) [URL: http://dx.doi.org/10.1117/1.JM3.13.1.013017.1].

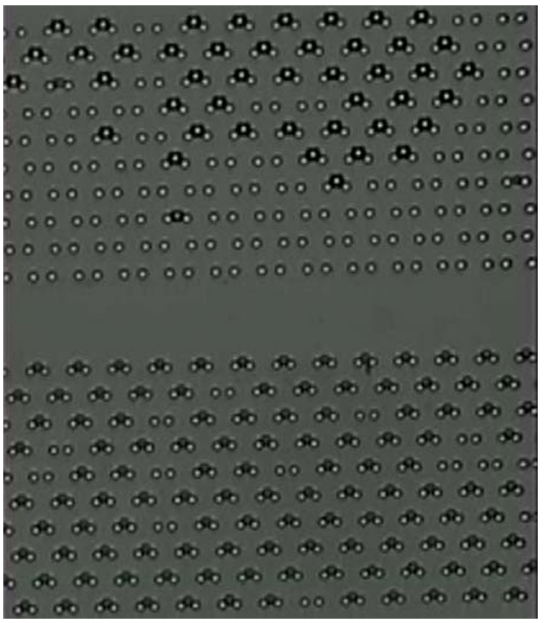

Video 2 The trapping processing of the large microspheres into the large trap region (MPEG, 2.69 MB) [URL: http://dx.doi.org/10.1117/1.JM3.13.1.013017.2].

microspheres overflow to the 5-μm trap region, they will encounter mostly filled 5-μm traps and thus use the bypass routes to escape the device. In the experiments, to simplify the device operation and improve the trapping performance, we control the microsphere concentration and volume to ensure that very few 7.7-μm microspheres overflow to the 5-μm trap region.

As for the packing density of our device, from Table 1, we compute the areas of the small trap and the large trap as 1102.2 and 1859.3 μm^2, respectively. The corresponding packing densities for the two trap areas are 907 and 537 traps/mm^2, respectively. Therefore, our device provides a much smaller unit cell area and thus much higher packing density compared with other designs.[32] Further more, in order to achieve its functions, it is important for the device to have high trapping efficiency, i.e., a single microsphere in one trap (single), and to avoid fluidic errors such as multiple microspheres in one trap (multiple), empty traps (empty), channel clogged by microspheres (clogged), and small microspheres captured in the large traps or large microspheres captured in the small traps (wrong-trapped). Figure 5 also provides the illustrative examples of single, multiple, empty, clogged, and wrong-trapped, highlighted in circles. Intuitively, for both small and large trap array regions, our device has large value for single but small values for multiple, empty, clogged, and wrong-trapped.

To further evaluate the performance of our device, we compute the fractions of traps for single, multiple, empty, and wrong-trapped and the fraction of channels for clogged at the end time points of the microsphere-trapping experiments. Figure 6 presents these performance measurements, which are computed separately for the small [Fig. 6(a)] and the large [Fig. 6(b)] trap arrays, based on the results of 10 fabricated devices. The standard deviations of these measurements for both trap array regions are small, which suggests that our experimental results are statistically representative and reproducible. For the small and large trap regions, single is dominant (96.64% and 91.25%, respectively), and the undesired multiple is negligible (1.20% and 2.42%). The percentage of empty is close to 0% for the small trap arrays, indicating that almost no small traps remain empty at the end. As long as the small microspheres can find paths to reach the empty traps, they will eventually fill the empty traps. However, empty is a bit higher (4.08%) for the large trap arrays, because we intentionally limit the total number of large microspheres to avoid overflow. Moreover, the observed clogged (0% and 0.58%) and wrong-trapped (0.54% and 0.63%) are also negligible for the small and the large trap arrays, given that we carefully controlled the concentrations of the two-sized microspheres.

In summary, the microsphere-trapping experiments successfully demonstrate the high efficiency and few fluidic errors of our microfluidic microsphere-trap array device in trapping microspheres of two sizes, which paves the way for the application of this device for simultaneous detection of two types of targets. However, our design is not limited to detecting two target types. By changing the number n of microspheres and providing the microspheres' radius in the design framework in Eqs. (1)–(8), we can build the device for simultaneous detection of more targets.

3.5 *Discussion*

In the design of our device, we considered the randomness of the microsphere size and incorporated it into our optimization framework. While the size variation of microspheres is

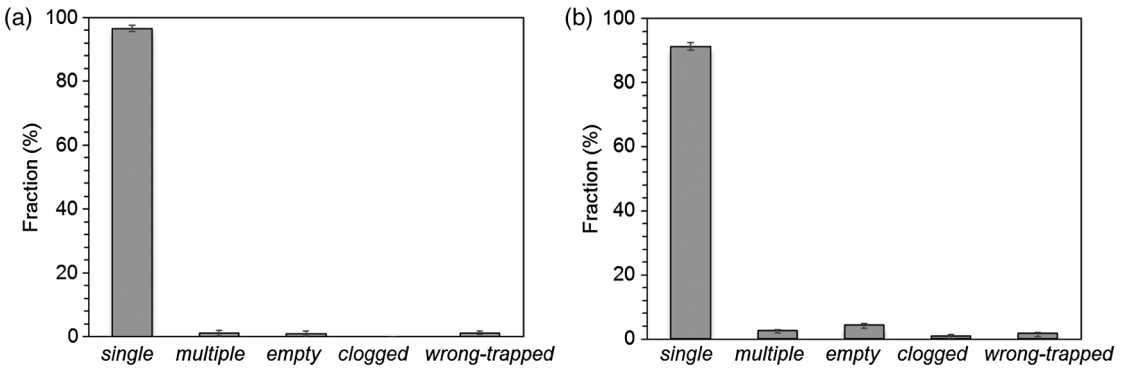

Fig. 6 Device performance for the sequential loading and trapping of (a) the 5-μm microspheres and (b) the 7.7-μm microspheres at the end time points of the experiments. The reported values are averaged results obtained on 10 devices, and the error bars indicate the standard deviations of the results.

small, the consideration may not affect much of the design results; the consideration can be of great importance when designing the device for cells that have a rather wide size distribution.

In the experiments, we used sequential loading of two different-sized microspheres into the device to minimize trapping errors. Ideally, if we can mix the two microspheres and load them simultaneously into the device, then simpler and scalable device operation can be achieved. In our preliminary experiments with this approach, we found that it is more difficult to achieve error-free trapping. This is due to the fact that with mixed loading, we can no longer guarantee the preferred 5-μm first loading sequence because larger microspheres can overflow to smaller microsphere trap area due to the finite chip size, resulting in misplaced microspheres. However, further investigation is needed to confirm this hypothesis and to help design better trap structures in order to achieve simultaneous mixed loading. One possible solution is to ensure that the larger microspheres never (or rarely) overflow to the smaller trap area by increasing the number of larger traps if the application allows; although this may lead to less efficiently utilized larger traps. Better solutions will be to spatially separate the different-sized traps and use hydrodynamic metamaterials, such as deterministic lateral displacement structures,[33,34] to direct different-sized microspheres to the corresponding optimized trap areas.

We demonstrated our design using a device for simultaneous detection of two types of biomolecules, in finite element simulations and experiments. However, as formulated in Sec. 2, our design generally works for low-level multiplex biomolecule detection (n up to 5); the number of types is limited by the number of commercially available microsphere sizes and the size uniformity. Given the number of target types n and the carefully selected radius R_i $(i = 1, \ldots, n)$ of the microspheres to capture the targets, we can obtain the geometric parameters $\boldsymbol{\delta}_i$ $(i = 1, \ldots, n)$ of our device by solving the optimization problems in Eqs. (1)–(8).

We proposed the device to immobilize microspheres for capturing and detecting multiple biomolecules such as mRNAs and proteins. However, according to the structure and hydrodynamic trapping mechanism of the device, we also believe that the device can be utilized for label-free approaches to identify, isolate, and enumerate cells of different sizes including circulating tumor cells and blood cells.[21–24] To achieve these goals, however, further development of the device is required to solve issues such as blood clogging, cell deformation, etc.

4 Conclusions

We developed an analytical framework to build a microfluidic microsphere-trap array device for simultaneous, efficient, and accurate detection of multiple targets in a single channel. We proposed to immobilize microspheres of different sizes at different regions in the channel of the device. These different-sized microspheres are to capture different targets and further identify the targets based on their positions. We extended our previous optimization framework for optimal design of this device. To demonstrate our design, we built a device for trapping microspheres of two different sizes for detection of two types of targets and validated the design by finite element fluidic dynamics simulations. We also fabricated the device and performed microsphere-trapping experiments to evaluate its performance. The results showed that our device achieved the position encoding of the microspheres with high efficiency and few fluidic errors. Thus, the device is advantageous in easy fabrication, convenient operation, and efficient detection of multiple targets.

We are currently applying our device to simultaneously detect epithelial growth factor receptor (EGFR) protein and mRNA, commonly overexpressed in cancers of breast, lung, colon, etc.[35] Overexpression of EGFR correlates with a poor prognosis and therefore carries significant predictive value in its quantification. Based on the results using our device, we are estimating EGFR and EGFR mRNA expression levels and performing correlation analysis to accurately determine the significant values necessary for early detection of cancer. The device can be utilized to separate, sort, or enumerate cells, such as circulating tumor cells and blood cells, based on cell size and deformability. Therefore, the device is promising to become a cost-effective and point-of-care miniaturized disease diagnostic tool.

Acknowledgments

This work was supported by National Science Foundation Grant No. CCF-0963742.

References

1. X. Xu et al., "Performance analysis and design of position-encoded microsphere arrays using the Ziv-Zakai bound," *IEEE Trans. Nanobiosci.* **12**(1), 29–40 (2013).

2. A. Mathur, "Image analysis of ultra-high density, multiplexed, microsphere-based assays," Ph.D. Thesis, Biomed. Eng., Northwestern University, Evanston, IL (2006).
3. J. R. Epstein et al., "High-density, microsphere-based fiber optic DNA microarrays," *Biosens. Bioelectron.* **18**(5–6), 541–546 (2003).
4. J. M. Schwenk and P. Nilsson, "Antibody suspension bead arrays," *Methods Mol. Biol.* **723**, 29–36 (2011).
5. C. Situma, M. Hashimoto, and S. A. Soper, "Merging microfluidics with microarray-based bioassays," *Biomol. Eng.* **23**(5), 213–231 (2006).
6. R. H. Liu et al., "Integrated microfluidic biochips for DNA microarray analysis," *Expert Rev. Mol. Diagn.* **6**(2), 253–261 (2006).
7. K. L. Gunderson et al., "Decoding randomly ordered DNA arrays," *Genome Res.* **14**(5), 870–877 (2004).
8. R. M. Dorazio and J. A. Royle, "Mixture models for estimating the size of a closed population when capture rates vary among individuals," *Biometrics* **59**(2), 351–364 (2003).
9. S. Rodiger et al., "A highly versatile microscope imaging technology platform for the multiplex real-time detection of biomolecules and autoimmune antibodies," *Adv. Biochem. Eng. Biotechnol.* **133**, 35–74 (2013).
10. W. J. Rhee and G. Bao, "Simultaneous detection of mRNA and protein stem cell markers in live cells," *BMC Biotechnol.* **9**(30), 1–10 (2009).
11. W. H. Grover et al., "Development and multiplexed control of latching pneumatic valves using microfluidic logical structures," *Lab Chip* **6**(5), 623–631 (2006).
12. T. Thorsen, S. J. Maerkl, and S. R. Quake, "Microfluidic large-scale integration," *Science* **298**(5593), 580–584 (2002).
13. S. Bohm et al., "A micromachined silicon valve driven by a miniature bi-stable electro-magnetic actuator," *Sens. Actuators A* **80**(1), 77–83 (2000).
14. M. Capanu, J. G. Boyd, and P. J. Hesketh, "Design, fabrication, and testing of a bistable electromagnetically actuated microvalve," *J. Microelectromech. S.* **9**(2), 181–189 (2000).
15. R. Pal et al., "Phase change microvalve for integrated devices," *Anal. Chem.* **76**(13), 3740–3748 (2004).
16. Z. Y. Li and D. Psaltis, "Optofluidic distributed feedback dye lasers," *IEEE J. Sel. Top. Quant.* **13**(2), 185–193 (2007).
17. R. Klemm et al., "Magnetic particle-based sample-prep and valveing in microfluidics," *Proc. SPIE* **8251**, 825108 (2012).
18. X. Xu et al., "Microfluidic microsphere-trap arrays for simultaneous detection of multiple targets," *Proc. SPIE* **8615**, 86151E (2013).
19. A. Karimi, S. Yazdi, and A. M. Ardekani, "Hydrodynamic mechanisms of cell and particle trapping in microfluidics," *Biomicrofluidics* **7**(2), 021501 (2013).
20. X. Xu et al., "Optimization of microfluidic microsphere-trap arrays," *Biomicrofluidics* **7**(1), 014112 (2013).
21. P. T. Lv et al., "Spatially gradated segregation and recovery of circulating tumor cells from peripheral blood of cancer patients," *Biomicrofluidics* **7**(3), 034109 (2013).
22. I. Cima et al., "Label-free isolation of circulating tumor cells in microfluidic devices: current research and perspectives," *Biomicrofluidics* **7**(1), 011810 (2013).
23. S. J. Tan et al., "Microdevice for the isolation and enumeration of cancer cells from blood," *Biomed. Microdevices* **11**(4), 883–892 (2009).
24. J. D. Chen et al., "A microfluidic chip for direct and rapid trapping of white blood cells from whole blood," *Biomicrofluidics* **7**(3), 034106 (2013).
25. A. Shapiro and A. Philpott, "A Tutorial on Stochastic Programming," http://www2.isye.gatech.edu/people/faculty/Alex_Shapiro/TutorialSP.pdf (2007).
26. J. Rice, *Mathematical Statistics and Data Analysis*, Duxbury Press, Farmington Hills (1995).
27. S. A. Campbell, *The Science and Engineering of Microelectronic Fabrication*, Oxford University Press, Oxford (1996).
28. P. Sarder and A. Nehorai, "Statistical design of position-encoded microsphere arrays," *IEEE Trans. Nanobiosci.* **10**(1), 16–29 (2011).
29. X. Xu, P. Sarder, and A. Nehorai, "Statistical design of position-encoded microsphere arrays at low target concentrations," in *2011 Conf. Record of the Forty Fifth Asilomar Conf. Signals, Systems and Computers (ASILOMAR)*, Pacific Grove, CA, pp. 1694–1698, IEEE (2011).
30. T. G. Kolda, R. M. Lewis, and V. Torczon, "Optimization by direct search: new perspectives on some classical and modern methods," *SIAM Rev.* **45**(3), 385–482 (2003).
31. X. Xu, Z. Li, and A. Nehorai, "Finite element simulations of hydrodynamic trapping in microfluidic particle-trap array systems," *Biomicrofluidics* **7**(5), 054108 (2013).
32. W. H. Tan and S. Takeuchi, "A trap-and-release integrated microfluidic system for dynamic microarray applications," *Proc. Natl. Acad. Sci. U. S. A.* **104**(4), 1146–1151 (2007).
33. L. R. Huang et al., "Continuous particle separation through deterministic lateral displacement," *Science* **304**(5673), 987–990 (2004).
34. K. J. Morton et al., "Hydrodynamic metamaterials: microfabricated arrays to steer, refract, and focus streams of biomaterials," *Proc. Natl. Acad. Sci. U. S. A.* **105**(21), 7434–7438 (2008).
35. R. I. Nicholson, J. M. Gee, and M. E. Harper, "EGFR and cancer prognosis," *Eur. J. Cancer* **37**(Suppl 4), S9–S15 (2001).

Xiaoxiao Xu is a PhD student in the Preston M. Green Department of Electrical and Systems Engineering at Washington University in St. Louis. She received the BSc degree in optical science and engineering from Fudan University, China, in 2009, and the MSc degree in electrical engineering from Washington University in St. Louis in 2011. Her current research interests include statistical signal processing, image processing, and genomic signal processing. She is a member of SPIE.

Zhenyu Li is an assistant professor in the ECE Department at George Washington University, where he leads the Nanophotonics and Microfluidics Laboratory. He received his PhD degree in electrical engineering from the California Institute of Technology (Caltech), in 2007. His research interests include nanophotonics, microfluidics, and their applications in biology and medicine.

Pinaki Sarder is a postdoctoral researcher in radiology at Washington University in St. Louis (WUSTL). His research is focused on integrated optical imaging using multi-photon microscopy, fluorescence molecular tomography, and statistical signal processing methods. He obtained his BTech degree in electrical engineering (EE) from the Indian Institute of Technology, Kanpur and the MSc and PhD in EE from WUSTL. His research contributions span across multiple disciplines including signal processing, optimization, microscopy, and optics.

Nalinikanth Kotagiri is a postdoctoral researcher in the Department of Radiology at Washington University School of Medicine. He received the MB, BS degree in general medicine from Andhra Medical College, India, in 2000 and the PhD degree in cell and molecular biology from the University of Arkansas, Fayetteville, in 2011. His current research interests are developing and demonstrating *ex vivo* and *in vivo* techniques to detect and estimate tumor biomarkers for early detection of cancer.

Arye Nehorai is the Eugene and Martha Lohman professor and chair of the Preston M. Green Department of Electrical and Systems Engineering, Washington University in St. Louis. He received his BSc and MSc degrees from the Technion, Haifa, Israel, and his PhD degree from Stanford University. He is a fellow of the AAAS, IEEE, and the Royal Statistical Society.